Exploring the Effects of Vegetation and Vegetation-Induced Topography on the Distributions of Near-Bed Flow Parameters

A Thesis
Presented in Partial Fulfillment of The Requirements for the
Degree of Master of Science
with a
Major in Civil Engineering
in the
College of Graduate Studies
University of Idaho
by

Caitlin Keady

Approved by:

Major Professor: Elowyn Yager, Ph.D.
Committee Members: Andrew Tranmer, Ph.D., James McNamara, Ph.D.
Department Administrator: Fritz Fiedler, Ph.D.

August 2022

Abstract

Vegetation is a vital component of river systems and impacts turbulence intensities, velocities, and shear stresses near the bed, which affect local bed topography. The near-bed flow field is influenced directly by vegetation and by vegetation induced topography. The relative importance of these two effects on spatial distributions of near-bed velocities, Reynolds stresses, and turbulent kinetic energies (TKE) are not well understood. We conducted laboratory flume experiments with a single stalk and flat bed, a single stalk with a scour hole, and a scour hole with no stalk to isolate the effects of vegetation and topography. We also used previously published data to test if equations for the spatially averaged patch velocity (U) and TKE ($\langle TKE \rangle$) in vegetated flat beds provided accurate predictions for vegetated natural bed topographies. Lastly, we determined if TKE distributions over vegetated natural topography can be simply predicted using mean patch velocity and an assumed gamma distribution. Equations designed for flat beds predicted mean patch velocity and mean near-bed turbulent kinetic energy well for low measured U and $\langle TKE \rangle$ in beds with natural topography and vegetation. Not all measured TKE data fit a gamma distribution well, however a relation may exist between vegetation density and the shape parameter of a two-parameter gamma distribution.

Acknowledgements

I would like to extend my appreciation for my advisor, major professor, and mentor Dr. Elowyn Yager for supporting me and guiding me through my graduate school experience, particularly through a pandemic. I would also like to thank Dr. Angel Monsalve, Dr. Jeff Reeder, Dr. Jaeho Shim, and Bob Basham for teaching, supervising, and answering my numerous questions throughout my time in the lab. I am also grateful for my office mates Jenna, Raine, Brandon, Andrea, and Taylor who always lent a helping hand and brightened my spirits. Finally, I would like to thank the Washington Department of Transportation and the National Cooperative Highway Research Program for funding me throughout my time at the University of Idaho.

Table of Contents

List of Figures

List of Tables

Introduction

Vegetation provides essential habitat for salmonids, regulates nutrient availability, and alters sediment transport regimes (Carpenter & Lodge, 1986, Kaufmann et al. 1999). Furthermore, vegetation can increase bank and channel stability, making it an important component of river systems (Pollen, 2007; Simon & Collison, 2002). In particular, rigid emergent vegetation impacts flow by changing means and distributions of near-bed, time-averaged velocities, turbulent kinetic energies (TKE), and Reynolds stresses (Nepf, 1999; Liu et al., 2008). However, vegetation induced flow changes can have competing potential effects on sediment transport and sedimentation within a patch. Vegetation generated turbulence may increase sediment transport, however vegetation also exerts drag on the flow, decreasing mean flow velocity, which could reduce sediment transport (Yang & Nepf, 2018, Rominger et al., 2010, Romdhane et al., 2018, Stoesser et al., 2010, Vargas-Luna et al., 2014). The relative importance of mean flow velocity and turbulence in controlling sediment transport may depend on the vegetation density.

Vegetation density or solid volume fraction (ϕ) can alter the shape and scale of the spatial distributions of near-bed, time-averaged streamwise velocity ($\overline{u}$); near-bed, time-averaged Reynolds stress; and near-bed, time-averaged TKE (Nepf, 2012; Wang et al., 2015). Vegetation density will also change the spatially averaged values of these parameters. Equations exist to predict mean flow parameters in vegetation patches, such as *U* and the time and space averaged near-bed TKE ($\langle TKE \rangle$), (Yang and Nepf, 2016; Yang and Nepf, 2018; King et al., 2012) as a function of ϕ but none predict the probability distributions for these parameters. For example, $\langle TKE \rangle$ can increase with greater vegetation density under constant patch averaged velocity (*U*; averaged through flow depth, patch width, patch length, and time) (Yager & Schmeeckle, 2013) however, the magnitude of the TKE distribution changes with vegetation density is not known. The spatial distribution of near-bed shear stresses around each individual stem is similar to what has been observed around cylindrical bridge piers (Etminam et al., 2018). Similarly, near-bed velocities spike in the immediate wake of stalks for sparse vegetation arrays (Neary, 2012; Rominger et al., 2010; Romdhane et al., 2018), which likely contributes to local erosion and deposition within an array

(Rominger et al., 2010; Romdhane et al., 2018; Vargas-Luna et al., 2014). Understanding how vegetation density impacts the spatial variability of stresses, velocities, and turbulent kinetic energies could be helpful to accurately predict local and channel wide sediment transport, nutrient mobility, and habitat availability (Neary, 2012; Liu et al., 2008; Stoesser et al., 2010; Wang et al., 2015).

Previous studies have demonstrated that sediment transport models based on time and space averaged shear stresses are not accurate in vegetation patches because of vegetation-generated turbulence (Yang & Nepf, 2018). Yang and Nepf (2018) proposed using $\langle TKE \rangle$ in sediment transport equations because $\langle TKE \rangle$ indirectly accounts for turbulence-induced sediment motion in vegetated patches. However, using $\langle TKE \rangle$ can potentially lead to inaccurate sediment transport predictions because of the large spatial variability of $\langle TKE \rangle$ in vegetation patches (Yager & Schmeeckle, 2013). Predictions of bedload transport through roughness fields may require using the distribution of shear stress or TKE rather than a single representative value such as the mean or median (Monsalve et al., 2016; Monsalve et al., 2020; Nicholas, 2000; Recking, 2013). Few studies have applied distributions of shear stress or TKE in vegetated channels to model sediment transport. However, using flow distributions rather than spatially averaged values can improve sediment transport predictions by capturing spatial variability in TKE or shear stress, particularly in vegetation patches, where these parameters vary substantially.

In addition to the direct influence of vegetation on flow, vegetation changes bed topography via local erosion and deposition around stalks. The presence of these topographic features, which are visually similar to bedforms, can increase the width of the velocity, TKE, and shear stress distributions and change turbulence and sediment transport regimes (Leary & Schmeeckle, 2016; Jerolmack, 2005; Tinoco et al., 2020). Bedforms such as dunes can initiate flow separation over their crests, which can cause high instantaneous velocities to move downward into the bed and outward in all directions where flow reattachment occurs. These splat events cause pressure differences in and near the bed and can result in local bedload transport (Leary & Schmeeckle, 2016). Splat events can also move dissolved oxygen, nutrients, and organic matter into the hyporheic zone to be used by microbes and

invertebrates (Boulton et al., 1998). Because vegetation creates more complex bed topography, it could potentially increase local bedload transport and nutrient cycling in a similar manner as a dune system without vegetation. Many studies on flow through vegetation have a flat bed rather than a naturally formed bed with more complex topography (Bennett et al., 2002; Tanino and Nepf, 2007; Liu et al., 2008; Yang et al., 2015) whereas other studies have measured the combined direct and indirect (i.e. vegetation induced topography) effects of vegetation on flow (Yager and Schmeeckle, 2013; Tinoco and Coco, 2018). The relative effects of vegetation and vegetation induced topography on flow are therefore not well understood.

To address these knowledge gaps, our study focuses on several research questions. How important is natural topography around vegetation when assessing the impacts of vegetation on the means and distributions of near-bed velocities, Reynolds stresses, and TKE? How well do equations for U and $\langle TKE \rangle$ derived from vegetated flat bed conditions perform in for flow over naturally complex topography with vegetation? Do the shape and scale of distributions of near-bed velocities, Reynolds stresses, and TKE vary with vegetation density? We conducted three experiments in a laboratory flume: one experiment with a flat bed and a rigid simulated vegetation stalk, one experiment with a scour hole around the simulated stalk, and one with a scour hole and no stalk. To eliminate the effects of wake interference and isolate the effects of each vegetation stalk, we used a single stalk in these experiments. Furthermore, we chose to focus on a scour hole rather than dunes or ridges because we found it to be the most prominent bedform present around a single stalk and in a vegetation patch. We also used data from experiments by Yager and Schmeeckle (2013) and tested mean flow equations from Yang and Nepf (2016), Yang and Nepf (2018), and King et al. (2012).

Design and Methodology

SPIV Experiments

We conducted three experiments in the University of Idaho Aquatic Imaging Flume in Boise, Idaho to assess the impact of vegetation and vegetation induced topography (scour) on various flow parameters and their distributions. One of our goals was to isolate the effects of vegetation and topography on near bed flow without the influence of nearby vegetation or topography. In order to isolate the impact of the stalk and the scour hole, we chose to conduct experiments with a single stalk and a scour hole rather than an array of vegetation to eliminate wake interference. The experiments were conducted in a 0.5 m wide x 7 m long flume with a slope of 0.001. Water entered the flume through a honeycomb grid to reduce bubbles and turbulence and exited the flume over a rectangular weir of height 0.029 m to establish uniform flow. A single simulated vegetation stalk was installed in the center of the flume and a scour hole was created (see below for details) around the stalk for select experiments. The three experiments had the following conditions: single stalk with a flat bed, single stalk with a scour hole, and a scour hole with no stalk. These experiments will be referred to as flat bed-stalk, scour hole-stalk, and scour hole-no stalk and they will collectively be referred to as the single stalk experiments hereinafter.

The flume was filled with glass particles (approximately 0.003 m in diameter) and simulated sediment made of THV (0.0029 m in diameter), a polymer composed of tetrafluoroethylene, hexafluoropropylene, and vinylidene fluoride. THV was selected for its density, optical clarity, and refractive index, which is relatively easy to match to water by adding magnesium sulfate (Epsom salt), thus enabling us to see through the bed to obtain images of the flow within the scour hole (Rubol et al., 2017). To improve the clarity of the THV particles, we heated them in an oven at a temperature of 115°C for 30 minutes, in a process called annealing. The particles had to be spread out (not touching each other) on a nonstick surface, therefore multiple rounds were required to reach the desired volume of 3.3 L to fill a 0.50 m long x 0.22 m wide x 0.03 m deep area located roughly in the center of the flume length (Figure 1). To save time, the glass particles were used to fill the remainder of the flume outside the experimental area.

Prior to each experiment, we filtered the water and matched the refractive index. by adding magnesium sulfate to the water in small quantities until the ideal ratio of water to salt was achieved such that the refractive index of the water-salt mixture measured 1.365, the same as the THV per manufacturer specifications. We tested possible flow conditions (discharge, velocity, depth) to ensure that the THV sediment would not move during the experiments, which was necessary because we needed the bed topography to remain stable throughout each run. We used a flow discharge of 0.0045 m^3/s with a velocity of 0.15 m/s, a depth of 0.06 m, and a reach averaged shear stress of 0.589 Pa.

For the two experiments with a scour hole, a mold was pressed into the bed around the stalk to replicate the shape of a stable scour hole obtained from an experiment in a larger flume. The larger flume experiment was completed in a 20.0 m long by 2.0 m wide flume with a slope of 1.15% (Budwig & Goodwin, 2012) using an armored gravel bed with a D_{16} of 9.3 mm, a D_{50} of 11.0 mm, and a D_{84} of 13.0 mm, representing the 16th, 50th, and 84th percentiles, respectively, of the grain size distribution. Water was run through the flume for 12 hours at a discharge of 9000 gpm to transport large grains, then the flow was lowered to 8000 gpm for an additional 4 hours to move fine sediment either downstream or into the subsurface to create the well-developed armor layer. A 0.112 m diameter cylinder was then added 15 m downstream from the flume entrance and flow was run for 10 hours at 5600 gpm with a shear stress of 19.2 Pa until the cylinder adjacent scour hole was maximized and stable at a depth of 0.104 m. Next, structure-from-motion photogrammetry in AgiSoft Metashape and ArcGIS was used to obtain a digital elevation model (DEM) of the bed and the scour hole. We used 220 photos to obtain the DEM, which had a resolution of 0.16 mm. The scour hole depth, cylinder diameter, and DEM from the large flume were scaled down by a factor of 0.25 (the ratio of small and large flume widths) and used to print a 3D foam mold to replicate the shape and features of the large scour hole in the smaller flume with THV particles. We did not replicate these larger flume experimental conditions exactly, but rather we used the results to obtain information about the bed topography around the cylinder. These large flume experiments only produced a scour hole and no other bedforms were present, which further justified our focus on a single scour hole.

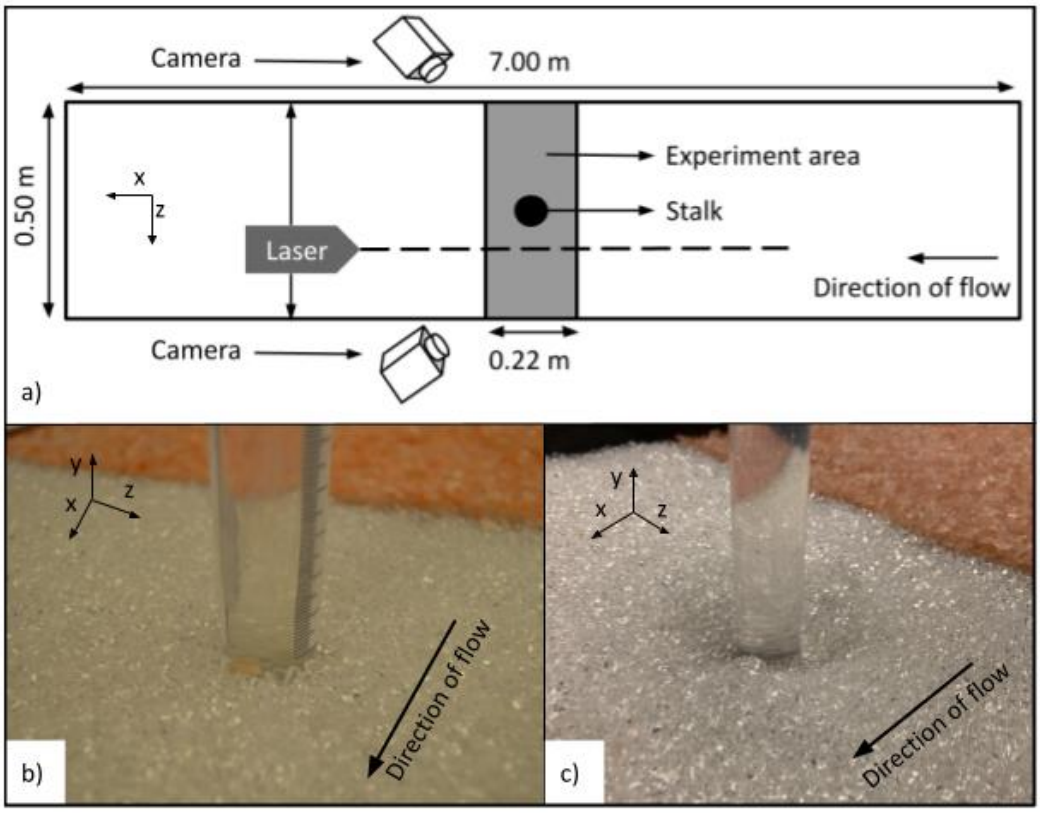

Figure 1 a) Experimental setup (not to scale) in the laboratory flume. b) Flat bed-stalk experimental setup. c) Scour hole-stalk experimental setup. White particles are THV and pink particles are glass.

The flat bed-stalk experiment consisted of a single rigid, emergent, hollow vegetation stalk made of THV with a diameter of 0.0254 m that was screwed into the bottom of the flume. The stalk was filled with water from the bulk flow to maintain the same refractive index through the stalk. The experimental area (0.50 m wide by 0.22 m long) was filled with THV particles and flattened by gently pressing a metal sheet onto the bed. The scour hole-stalk experiment had the same stalk as the flat bed-stalk experiment; however the scour hole mold was pressed into the bed around the stalk to create a scour hole modeled from the larger flume experiment. For the scour hole-no stalk experiment, the stalk was gently removed and the shape of the scour hole from the previous experiment was preserved. In each experiment, care was taken to ensure that the boundary between the glass grains and the THV grains was smooth and flat to prevent obstructions in the flow.

Yager and Schmeeckle (2013) performed an experiment with no vegetation and the distribution of all measured near-bed flow variables was very narrow, meaning that there was little spatial variation in these flow variables. Because the main goal in this paper is to examine flow distributions, comparison with a flat bed without vegetation would simply a show widening of flow variable distributions and would not contribute to the depth of our results.

In each experiment, we used 3D stereo particle image velocimetry (SPIV) with a dual laser system (two laser sheets coming from a single boroscope) that was fixed to a mobile cart above the flume, which allowed us to collect data at several streamwise transects across the flume. The boroscope was situated 0.5 m downstream from the vegetation stalk and the lasers were aimed upstream toward the stalk. The light sheets from the lasers were parallel to the walls of the flume and were moved between the right wall and the left wall to different transect locations (Figure 1). A computer on the mobile cart controlled the cross-stream location of the lasers, which ensured that the location of the light sheets in relation to the stalk was accurate and consistent between different experiments. Cameras were located outside of the flume on either side of the flume and were also fixed to the mobile cart. The field of view for the cameras was approximately 0.11 m upstream and 0.11 m downstream from the stalk and visualized the entire flow depth. The cameras were angled down at an angle of approximately 10°, however this angle varied slightly in each experiment and each transect because of the calibration process. The cameras were calibrated at each transect to maximize data quality. To calibrate the cameras, we focused them on a 3D calibration plate provided by LaVision to obtain the desired field of view and then calibrated using LaVision's Davis software. In each experiment, seeding particles were a mixture of 50 microns and 100 microns in diameter and were added to the water until they reached a density of 10^8 particles/m^2.

We measured 27, 27, and 24 transects for the flat bed-stalk, scour hole-stalk, and scour hole-no stalk experiments respectively. 2000 SPIV images were taken at each transect for each experiment over roughly 2 minutes at a rate of 16 frames/s. Transects were spaced 5 mm apart in the cross-stream direction to result in the combined transects spanning 10 cm on

either side of the vegetation stalk. We used transects within 10 cm of the stalk to focus on velocities that were directly influenced by the stalk and/or the scour hole. We identified interrogation regions (1x1 mm each) within each transect that were 1 cm above the bed. In some transects, the edges of the stalk obstructed the view of the seeding particles, resulting in erroneous velocities that were removed from the dataset. For the scour hole-stalk and scour hole-no stalk experiments, we had two additional closeup transects through the center of the stalk with the cameras adjusted at different angles with respect to the bed to ensure that we could see into the scour hole. However, we eliminated the closeup transect through the center of the scour hole for the scour hole-no stalk experiment because the image was tilted and cropped and because without the stalk, it was difficult to determine the location of the image within the field of view of the original transect at that location. In the scour hole-stalk experiment, the measurements in the closeup transect replaced those at the same locations in the original transect.

The SPIV data were processed to obtain time-average velocities ($\overline{u}$, $\overline{v}$, and $\overline{w}$), instantaneous velocities, and Reynolds stresses 1 cm above the bed in each transect, where *x, y,* and *z* represent streamwise, vertical, and cross stream directions respectively. The Reynolds stress was calculated as,

$$Re_{uv} = -\rho\overline{u'v'}, \tag{1}$$

where $u' = u - \overline{u}$, $v' = v - \overline{v}$ and $w' = w - \overline{w}$ and u, v, and w are instantaneous velocities. The density of water is represented by ρ, which is equal to 1000 for freshwater (experiments by Yager and Schmeeckle (2013)) and 1158 for the single stalk experiments due to the addition of salt. Turbulent kinetic energies were also calculated at 1 cm above the bed in each transect and experiment as,

$$TKE = \frac{1}{2}\left(\overline{(u')^2} + \overline{(v')^2} + \overline{(w')^2}\right) \tag{2}$$

Flow parameter distributions with vegetation & topography

We tested the fits of several probability distributions (stable, lognormal, extreme value, and gamma) but ultimately decided to pursue a gamma distribution to model the spatial distributions of the near-bed (1 cm above the bed) time-averaged velocities, Reynolds stresses, and TKE obtained from the SPIV data. We only discuss the results of the TKE distribution gamma fits because the velocity and Reynolds stress distributions did not fit a gamma distribution well. We selected a gamma distribution because it has been used in previous literature to model shear stress distributions (Monsalve et al., 2020; Nicholas, 2000; Recking, 2013) and because it is possible to estimate the scale parameter β from the shape parameter α. In addition, the other tested distributions did not fit any of the measured flow distributions well based on visual inspection. Specifically, we used a two-parameter gamma distribution,

$$f(x) = \frac{\beta^{\alpha} x^{\alpha-1} e^{-\beta x}}{\Gamma(\alpha)} \tag{3}$$

where $\beta = \alpha/\langle x \rangle$ (Monsalve et al., 2020). We used the Kolmogorov-Smirnov test (KS test) to assess the goodness of fit of the gamma distribution with TKE distributions from the single stalk experiments. The KS test compares whether the measured TKE are statistically from the same continuous distribution as the reference gamma distribution Our goal was to determine if the measured TKE distributions exhibited differences in α and β values with the addition or removal of a stalk or a scour hole.

Flow parameter distributions with changing vegetation density

Our next goal was to determine if α and β for each near-bed flow variable changed with solid volume fraction (ϕ) and *U*. Given that we did not vary ϕ or *U* in our experiments, we used the time-averaged, near-bed velocities ($\overline{u}$), Reynolds stresses, and TKE obtained from experiments conducted by Yager and Schmeeckle (2013). Again, we tested the fits of several probability distributions but selected a two-parameter gamma distribution (equation 3) to model these distributions. We also used the KS test to assess the goodness of fit of the gamma distribution with measured TKE distributions from Yager and Schmeeckle (2013).

Yager and Schmeeckle (2013) conducted 12 flume experiments in an 8.5 m long by 30.4 cm wide flume with a 0.5 mm sand bed. Vegetation was simulated with rigid, emergent cylinders in staggered arrays with varying densities. The simulated vegetation had a diameter of 1.3 cm and densities ranged from 0% to 4% vegetation density by area (ϕ = 0.006 - 0.031). The slope of the bed varied between 0.001-0.006, the flow discharge varied between 7.6E-03 m^3/s and 1.5E-02 m^3/s, and reach averaged shear stresses ranged from 0.23 Pa to 9.8 Pa. In each experiment, near bed (0.5 cm above the bed) streamwise and vertical velocities were measured using 2D PIV in three streamwise transects located through the center of two vegetation stalks and halfway between two vegetation stalks. A camera on the side of the flume recorded the laser sheet at 250 frames/s for approximately 19 s at each transect. To calculate TKE from measured velocities from Yager and Schmeeckle (2013), we used

$$TKE = \left(2\overline{u'^2} + \overline{v'^2}\right)/2 \tag{4}$$

(Yang et al., 2016). Equation 4 is a 3D approximation for TKE using only streamwise and vertical velocity components (Tanino and Nepf, 2007) for when the cross-stream velocity component is not available. See Yager and Schmeeckle (2013) for further details on these experiments.

Testing published equations for U and $\langle TKE \rangle$

To assess how well published equations estimate *U* and $\langle TKE \rangle$ in the single stalk experiments and in experiments by Yager and Schmeeckle (2013), we tested equations from Yang & Nepf (2018) and King et al. (2012). Space and time averaged flow velocity within a vegetation array, *U*, from Yang & Nepf (2018) was calculated as

$$U = \frac{ghS}{C_f + C_D\, ah/2}^{\frac{1}{2}} \tag{5}$$

where *g* is the acceleration due to gravity, *h* is the flow depth, *S* is the bed surface slope, *a* is the volumetric frontal area (*a* = *nd*), *n* is the number of plants per unit area, *d* is the stem diameter, and C_f is the bed friction coefficient calculated from Yang & Nepf (2018) as

$$C_f = \frac{1}{\left[5.75\log\left(\frac{2h}{d_s}\right)\right]^2} \quad (6)$$

where d_s is the sediment size and was 2.9 mm in our single stalk experiments and 0.5 mm in Yager and Schmeeckle (2013). Finally, the drag coefficient, C_D, varied with ad, according to Nepf (1999), and ranged from 1.10 to 1.13. We also tested the assumption that C_D was fixed at 1.0 (Yang & Nepf, 2018). Space and time averaged flow velocity within a vegetation array, U, from King et al. (2012) was calculated as

$$U = \left(\frac{2gS\,(1-\phi)}{C_D\,a}\right)^{\frac{1}{2}} \quad (7)$$

where $\phi = n\,\pi\,d^2/4$. Values of U were calculated using equation 5 and 7 for each of 12 experimental conditions in Yager and Schmeeckle (2013) and compared to measured values of U to determine how well these equations performed with varying vegetation density, discharge, and velocity conditions. We also predicted U for the flat bed-stalk and scour hole-stalk experiments to determine if the scour hole influenced the accuracy of equations 5 and 7. Next, we compared calculated and measured values of $\langle TKE \rangle$ from Yang and Nepf (2018) (modified from Yang and Nepf (2016)) as

$$\langle TKE \rangle = \frac{C_f}{0.19}\,U^2 + 0.9\,C_D^{\frac{2}{3}}\,\phi^{\frac{2}{3}}\,U^2 \quad (8)$$

where three different U values were tested for each experiment in equation 8: that calculated with equations 5 or 7, or the measured value. For U and $\langle TKE \rangle$ from Yager and Schmeeckle (2013) measured and predicted values were compared using the root mean squared error (RMSE).

To calculate ϕ for our single-stalk experiments, we assumed n = 25 stalks/m^2, which is based on the assumption that the stalk influences the flow in a surrounding area the size of the scour hole. The scour hole extended roughly 10 cm on either side of the stalk; thus, the stalk significantly influenced the flow near the bed within 10 cm on either side. Therefore, if the

single stalk existed in a vegetation patch, the stalks in the patch would need to be at least 20 cm apart for each stalk to be relatively isolated as occurred in our experiments. This assumption allowed for 25 hypothetical stalks to exist within one square meter without influencing the flow around one another. This is the maximum density possible, and this assumption was necessary to put our single stalk experiments in context with other experiments on vegetation patches.

Results

The near bed (1 cm above the bed) time averaged streamwise velocity ($\overline{u}$) measurements from the single stalk experiments revealed a variable spatial velocity distribution with generally higher velocities further from the stalk and lower velocities near the stalk and particularly in the wake of the stalk (Figure 2). High $\overline{u}$ values are present in the immediate left and right sides of the stalk, which could potentially contribute to scour and turbulence. Note that the reflection of the edges of the stalk can be seen in transects that do not go through the stalk (top and bottom of Figure 2) and these data were removed from the dataset for analysis.

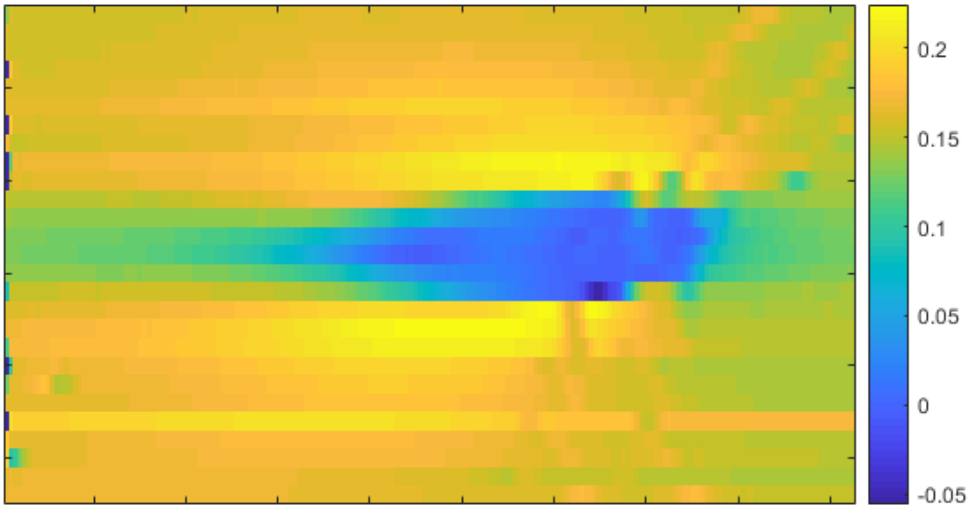

Figure 2 "Birds eye" view of $\overline{u}$ in the experiment area of the single stalk experiments. Colorbar indicates velocity (m/s) and flow travelled from right to left.

Testing published equations for U and $\langle TKE \rangle$

Equation 7 (King & Tinoco, 2012) predicted *U* well (RMSE = 0.041 m/s) for data from Yager and Schmeeckle (2013) and all predicted velocities were within a factor of two of the measured values (Figure 2). Predicted *U* had the highest accuracy for vegetation patches with ϕ = 0.013 and ϕ = 0.031 but were systematically greater than the measured values for ¾ of the experiments with ϕ = 0.006. In addition, equation 7 tended to overpredict *U* for high measured velocities and underpredict for low measured velocities. Equation 5 (Yang & Nepf, 2018) had a similar outcome as equation 7 (King & Tinoco, 2012), however it predicted *U*

from experiments by Yager and Schmeeckle (2013) slightly better overall (RMSE = 0.035 m/s) . Prediction accuracy for *U* was similar between the single stalk experiments and from data by Yager and Schmeeckle (2013), however equation 5 slightly underpredicted *U* and equation 7 slightly overpredicted *U* for the single stalk experiments. There did not appear to be a significant difference in equation 5 and 7 accuracies between the flat bed-stalk and scour hole-stalk experiments.

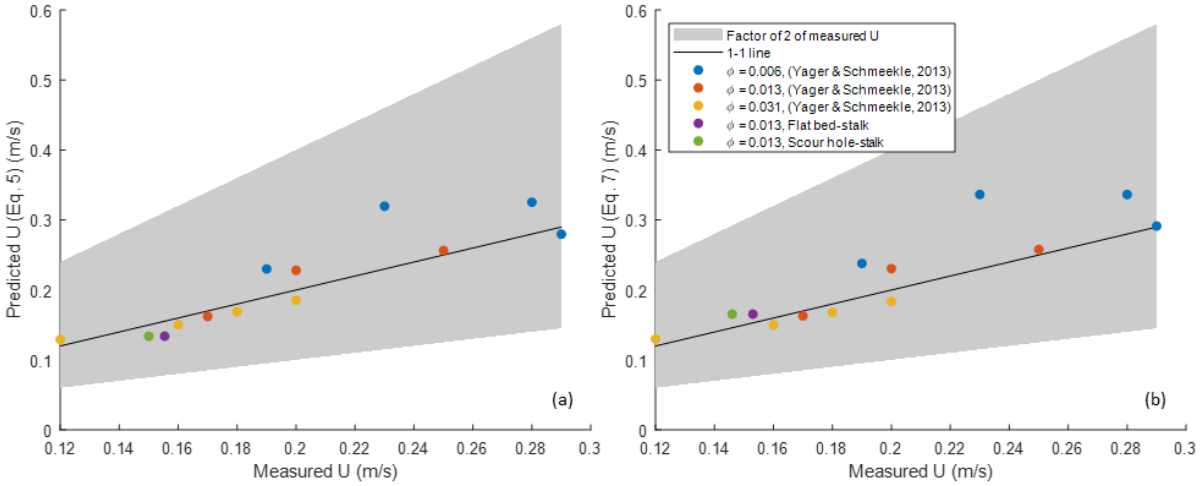

Figure 3 Relation between measured and predicted patch-averaged velocity using a) equation 5, b) and equation 7. The shaded region highlights predictions within a factor of two of the measured *U*.

When using the measured *U* in Yager and Schmeeckle (2013), equation 8 (Yang & Nepf, 2018) underpredicted $\langle TKE \rangle$ for high measured $\langle TKE \rangle$ and predicted $\langle TKE \rangle$ relatively well for low measured $\langle TKE \rangle$ (RMSE = 19.2 $(cm/s)^2$) (Figure 3a). When applying equation 8 with estimated *U* from equations 5 and 7, the RMSE values declined to 14.5 $(cm/s)^2$ and 14.0 $(cm/s)^2$, respectively (Figure 3b, 3c), however this could result from inaccurate estimates of *U* (Figure 2). Equation 8 also underpredicted $\langle TKE \rangle$ for high measured $\langle TKE \rangle$ and predicted $\langle TKE \rangle$ relatively well for low measured $\langle TKE \rangle$ when using estimated *U* from equations 5 and 7. There did not appear to be a strong connection between vegetation density and accuracy of $\langle TKE \rangle$ predictions in any application of equation 8 (Figure 3 a-c). All predictions of $\langle TKE \rangle$ for experiments by Yager and Schmeeckle (2013) was within a factor of two of the measured values (shaded region, Figure 3). Using measured *U*, equation 8 performed better for the

scour hole-stalk experiment than for the flat bed-stalk experiment. The scour hole-stalk predicted $\langle TKE \rangle$ was within a factor of two of the measured value and the flat bed-stalk predicted $\langle TKE \rangle$ was outside of this range (Figure 3).

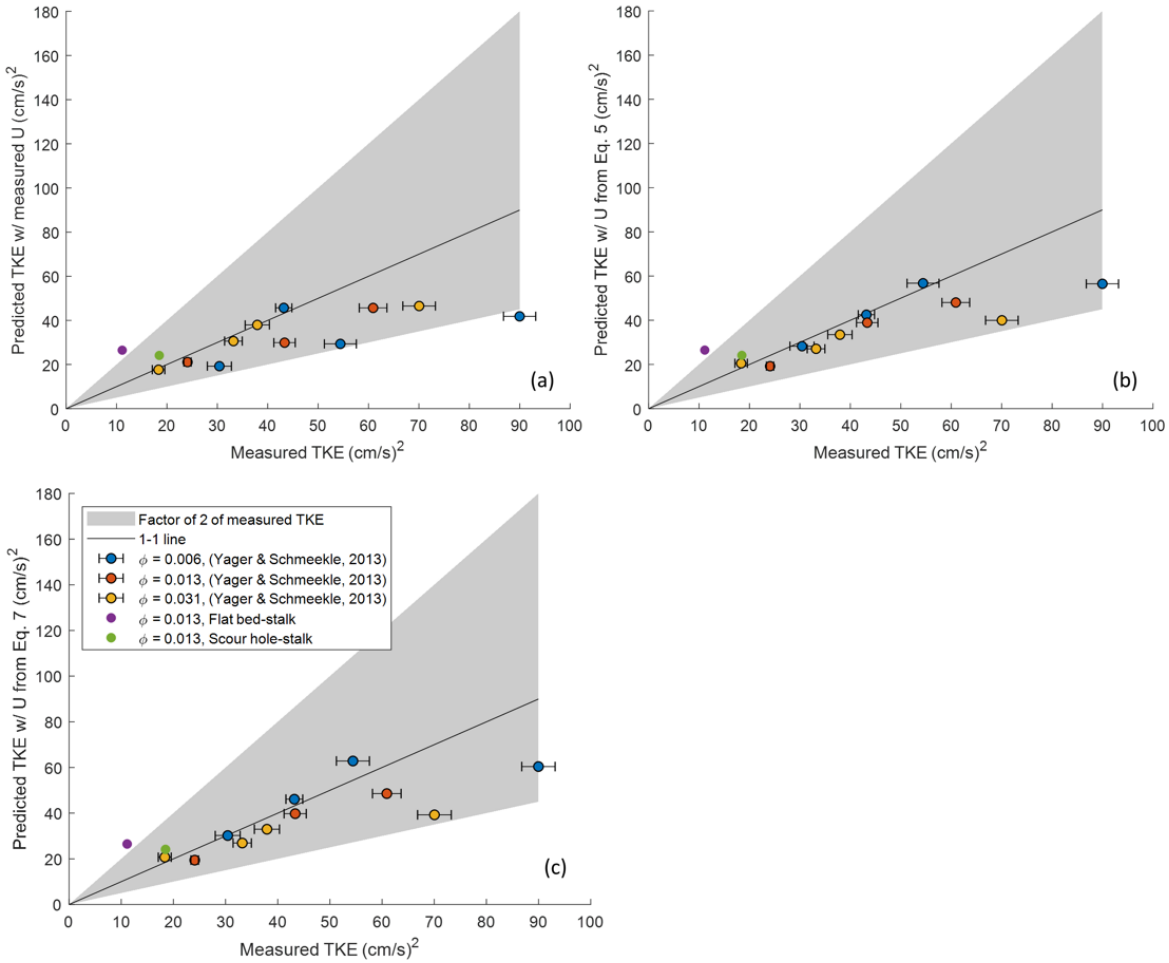

Figure 4 Relation between measured $\langle TKE \rangle$ and predicted $\langle TKE \rangle$ from Eq. 8. Predicted $\langle TKE \rangle$ was calculated with a) measured *U*, b) estimated *U* from Eq. 5, and c) estimated *U* from Eq. 7. Error bars represent the standard error and if not visible, they are within the symbol size. The shaded region indicates the area within a factor of two of the measured $\langle TKE \rangle$.

Flow parameter distributions with vegetation & topography

We first compared the spatial averages of the near-bed time-averaged streamwise velocities ($\overline{u}$), Reynolds stresses, and TKE between each of the three single stalk/scour hole experiments. We were focused on the interactions between the scour hole and stalk rather

than the individual effects of each compared to a flat bed because both scour holes and stalks are present in vegetation patches. In other words, we were interested in the importance of topography in the presence of vegetation rather than the influence of topography or vegetation alone. The presence of a scour hole slightly lowered the mean $\overline{u}$ from 0.155 m/s (flat bed-stalk) to 0.150 m/s (scour hole-stalk) and lowered the mean Reynolds stress from -0.093 Pa (flat bed-stalk) to -0.110 Pa (scour hole-stalk). $\langle TKE \rangle$ increased with the presence of a scour hole from 11.133 $(cm/s)^2$ (flat bed-stalk) to 18.485 $(cm/s)^2$ (scour hole-stalk). The presence of the stalk increased mean $\overline{u}$ from 0.127 m/s (scour hole-no stalk) to 0.150 m/s (scour hole-stalk) and increased mean Reynolds stress from -0.121 Pa (scour hole-no stalk) to -0.110 Pa (scour hole-stalk). The presence of the stalk increased $\langle TKE \rangle$ from 16.866 $(cm/s)^2$ in the scour hole-no stalk experiment to 18.485 $(cm/s)^2$ in the scour hole-stalk experiment.

The probability distributions for $\overline{u}$ within 10 cm of the stalk had different shapes between the three experiments. The two experiments with a stalk both had a small peak in the proportions of velocities that were slightly greater than $\overline{u}$ = 0 m/s, indicating a relatively high proportion of very low velocities. The absence of the stalk (scour hole-no stalk experiment) caused this feature of the distribution to disappear (Figure 4). In other words, the stalk caused many near zero velocities regardless of the presence of the scour hole. The proportion of velocities in the experiment without a stalk experiment steadily increased between 0.05 m/s and 0.13 m/s until it reached a peak value at moderate-high velocities. In the two experiments with a stalk the proportion of velocities did not increase steadily because it had two distinct peaks at moderate-high velocities. The scour hole-stalk experiment had a lower probability of low and medium velocities (0.05 - 0.12 m/s) than the scour hole-no stalk experiment, thus the presence of the stalk increased the proportion of low (except near 0 m/s) and medium velocities. The presence of the scour hole changed the shape of the distribution to have a sharper increase toward the mode and reduced the proportion of higher $\overline{u}$ values over 0.18 m/s.

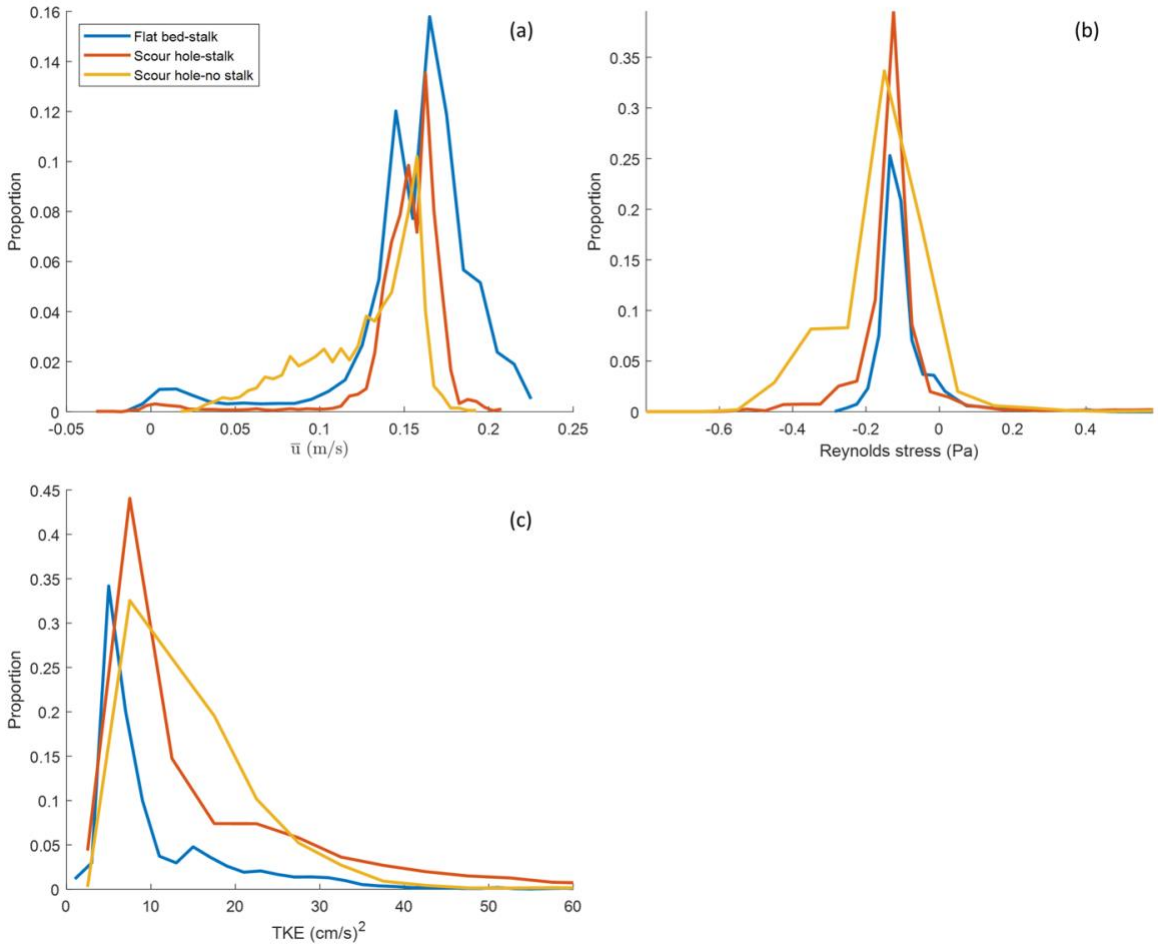

Figure 5 Time averaged near-bed a) velocity ($\overline{u}$), b) Reynolds stress, and c) TKE distributions as proportions for the single stalk and scour hole experiments.

When comparing the scour hole-stalk and scour hole-no stalk experiments, the presence of the stalk significantly narrowed the Reynolds stress distribution by reducing the proportions of both high and low Reynolds stresses. However, when comparing the flat bed-stalk and scour hole-stalk experiments, the presence of the scour hole only changed the distribution shape moderately, by increasing the proportion of stresses near the mode and slightly widening the distribution.

The presence of the scour hole in the scour hole-stalk experiment widened the TKE distribution and increased the proportion of moderate and high TKE compared to the flat

bed-stalk experiment. The presence of the stalk in the scour hole-stalk experiment narrowed the TKE distribution and increased the proportion of medium TKE values compared to the scour hole-no stalk experiment (Figure 4). Both experiments with stalks had a similar TKE distribution shape, with a distinct peak at low TKEs and a small local maximum for moderate TKE, unlike the TKE distribution for the scour hole-no stalk experiment, which had an overall greater proportion of moderate TKE and only had one peak.

Table 1. Summary of the results of the Kolmogorov-Smirnov test on TKE distributions from experiments by Yager and Schmeekle (2013) and the single stalk experiments.

Experiment		P-value
Experiments by Yager and Schmeeckle (2013)	ϕ = 0.013	0.95747
	ϕ = 0.013	0.98517
	ϕ = 0.013	0.98517
	ϕ = 0	0.6974
	ϕ = 0.006	0.78642
	ϕ = 0.006	0.98517
	ϕ = 0.006	0.97479
	ϕ = 0.006	0.80956
	ϕ = 0.031	0.048598
	ϕ = 0.031	0.78642
	ϕ = 0.031	0.6725
	ϕ = 0.031	0.023078
Single stalk/scour hole experiments	Flat bed-stalk	0.010793
	Scour hole-stalk	0.00048593
	Scour hole-no stalk	4.3362e-14

The measured probability density distributions of $\overline{u}$, near-bed time-averaged Reynolds stresses, and TKE for all three experiments were fit to a two-parameter gamma distribution (equation 3, Figure 5b). As mentioned in the methods, $\overline{u}$ and the near-bed time-averaged Reynolds stress probability density distributions were not well fit by any tested theoretical distribution. We found that the gamma distributions did not fit the measured TKE probability density distributions very well as all three experiments failed the KS test at a 5% significance level (p-value = 4.3E-14 - 0.012). However, the scour hole-no stalk experiment TKE probability density distribution visually seems to fit a gamma distribution well, except that the gamma distribution does not capture the peak density correctly.

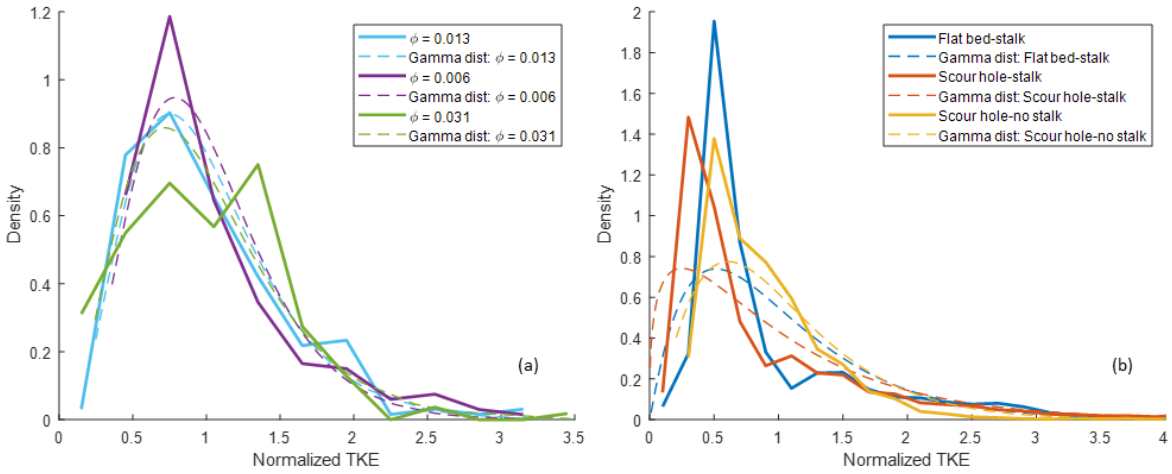

Figure 6 Distributions of TKE normalized by the spatially averaged value from each experiment from a) a representative sample of experiments by Yager and Schmeeckle (2013) and b) the single stalk and scour hole experiments. Gamma fits are shown with dotted lines.

Flow parameter distributions with changing vegetation density

Two parameter gamma distributions fit the TKE probability density distributions from Yager and Schmeeckle (2013) well (Figure 5a), with all but two experiments passing the KS test at a 5% significance level (p-value = 0.02 - 0.99). TKE probability density distributions from these experiments also visually fit gamma distributions well with a few minor exceptions, for example the ϕ = 0.031 case in Figure 5a did not fit a gamma distribution as well as the examples for ϕ = 0.006 and 0.013. The shape of the gamma distribution is controlled by α and lower α resulted in high probability densities at low TKE and higher α resulted in high probability densities at medium to high TKE and a more normal distribution shape. The scale

of the gamma distribution is controlled by β and higher β created a wider distribution. We expected α and β to increase with increasing *U* because higher *U* should increase TKE, which would shift the peak of the distribution toward higher TKE, which corresponds with an increase in α. Increases in both α and β would result in a more normal looking distribution of relatively high TKE with a longer right tail. We expected a similar outcome with increasing vegetation density because more stalks should produce higher TKE due to the increased flow complexity, however we expected higher vegetation density to correspond to a wider TKE distribution. Wider distributions, especially those with long right tails should increase sediment transport because of increased proportions of high TKE, which is a driver of sediment transport.

Although TKE probability density distributions from experiments by Yager and Schmeeckle (2013) were modelled relatively well with a gamma distribution, we did not find a single relation between α and *U* for all vegetation densities combined (Figure 6). Recall that we can calculate β as $\beta = \alpha/\langle x \rangle$ so we are only seeking to find a relation between α and *U* because we could use that α combined with $\langle TKE \rangle$ (measured or predicted using equation 8) to obtain β. We separated the results by vegetation density, and ϕ = 0.006 and 0.031 vegetation patches showed a positive relation between the α and *U*, however the ϕ = 0.013 vegetation patch had a negative relation. We also added data from the single stalk experiments for the flat bed-stalk and scour hole-stalk cases and they showed a similar positive relation between the α and *U* as the ϕ = 0.006 and 0.031 vegetation patches. It is important to note that these did not have the same experimental conditions (one had a scour hole and one did not) so it is difficult to determine if changes in *U* or the scour hole or a combination of both is driving this result. In addition, for a given *U*, α tends to increase with increasing ϕ, however the ϕ = 0.013 experiments from Yager and Schmeeckle (2013) were again the exception. We were unable to collapse all experiments into one reliable relation to predict α and β for a gamma distribution from *U* and ϕ.

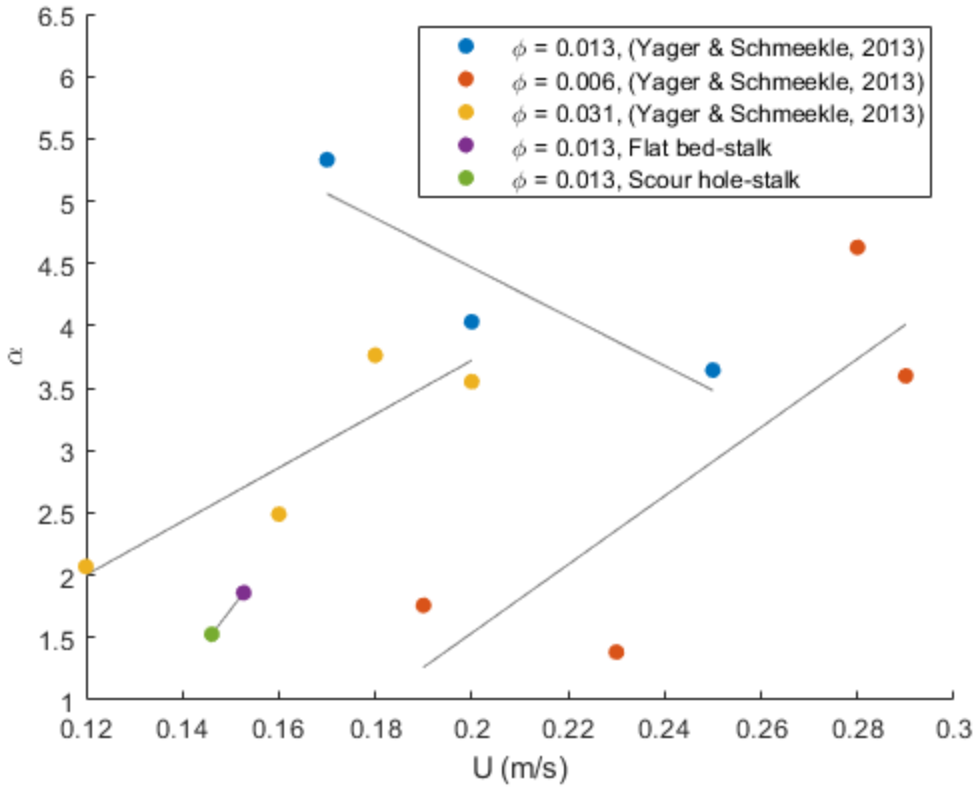

Figure 7 Relation between U and α for varying vegetation densities using data from experiments by Yager and Schmeeckle (2013) and data from the single stalk experiments.

Discussion

Testing published equations for U and $\langle TKE \rangle$

Equations 5 and 7 predict *U* well for beds with vegetation and natural topography, however the predictions for $\langle TKE \rangle$ using equation 8 were not always as accurate. Yang and Nepf (2016) used a flat sand bed to develop equation 8, where sand was glued to the bed surface to restrict sediment movement to only a thin layer of mobile grains, which ensured that no topography could form. Naturally complex topography was present in experiments by Yager and Schmeeckle (2013), which could have contributed to often underpredicted $\langle TKE \rangle$. Equations 5 and 7 also were not specifically developed for beds with natural topography, however the results of the single stalk experiments indicated that equations 5 and 7 predicted *U* well for flat beds (flat bed-stalk experiment) and beds with topography (scour hole-stalk experiment). Interestingly, Equation 8 predicted $\langle TKE \rangle$ better for the scour hole-stalk experiment than for the flat bed-stalk experiment, however more data are needed to confirm this finding because we assumed the maximum possible ϕ of these experiments, which is a parameter in equation 8. Decreasing the vegetation density for the single stalk experiments from ϕ = 0.013 to ϕ = 0.005 decreased TKE predictions (equation 8) and increased their accuracy when using *U* from equations 5 and 7. Vegetation density could be responsible for differences in accuracy between the flat bed-stalk and scour hole-stalk experiments rather than differences in bed topography.

Note that when applying equations 5, 7, and 8 to experiments by Yager and Schmeeckle (2013), we could not isolate the effects of topography, so we do not know the relative effects of the scour holes and stalks on the predictions of *U* and $\langle TKE \rangle$. Lastly, the single stalk experiments had a significantly higher measurement density in the scour hole than did the experiments by Yager and Schmeeckle (2013), which had some measurements in scour holes but also many measurements on topographic highs and depositional areas. We expected higher $\langle TKE \rangle$ in the scour hole, so these differences in measurement density and location could help to explain why equation 8 tended to underpredict $\langle TKE \rangle$ for the single stalk experiments and overpredict $\langle TKE \rangle$ for experiments by Yager and Schmeeckle (2013). In other words, the single stalk experiments had more measurements in the scour hole and a

high $\langle TKE \rangle$ that equation 8 underpredicted while the experiments by Yager the Schmeeckle (2013) had more measurements outside of the scour hole and lower $\langle TKE \rangle$ that equation 8 overpredicted.

Yang and Nepf (2018) used a range of vegetation densities to develop equation 5 (ϕ = 0.006 - 0.050), which is a similar range of ϕ (ϕ = 0.006 - 0.031) to what was used in experiments by Yager and Schmeeckle (2013). King and Tinoco (2012) used a higher range of vegetation densities (ϕ = 0.010 - 0.079) to develop equation 7. Equations 5 and 7 were generally more accurate for the ϕ = 0.013 and ϕ = 0.031 vegetation patches than the ϕ = 0.006 vegetation patch. The smallest prediction accuracy for the lowest density vegetation patch (ϕ = 0.006) could be because this patch had a lower ϕ than what was used to develop equation 7 or was at the lower limit of ϕ used to develop equation 5. Equation 8 was not as affected by vegetation density. Yang and Nepf (2016) published a more general version of equation 8 and tested it for ϕ = 0 - 0.050. This equation in Yang and Nepf (2016) predicted $\langle TKE \rangle$ well for ϕ = 0 and ϕ = 0.050, however it overpredicted $\langle TKE \rangle$ for ϕ between ϕ = 0 - 0.050. This general equation and equation 8 were modified from an equation in Tanino and Nepf (2008) for vegetation-generated turbulence, which was developed with ϕ = 0.01 - 0.35 vegetation patches in flat beds. This range of ϕ from Tanino and Nepf (2008) is on the higher end of the ϕ values studied in Yager and Schmeeckle (2013). The high ϕ values that equation 8 was developed with likely resulted in overlapping wakes within the vegetation patch, which could have influenced $\langle TKE \rangle$ more than the wake interference in experiments by Yager and Schmeeckle (2013). This difference in wake interference was indirectly associated with vegetation density and could have contributed to some of the overpredictions in Equation 8 (Figure 3).

Equations 5, 7, and 8 were more accurate for lower measured values of *U* and $\langle TKE \rangle$ and became less accurate for high measured values of *U* and $\langle TKE \rangle$. Therefore, it could also be possible that these equations are limited by flow range rather than by the presence of topography or vegetation density. Yang and Nepf (2016) tested the more general version of equation 8 with measured $\langle TKE \rangle$ that were significantly lower (~9-16 $(cm/s)^2$) than the $\langle TKE \rangle$ in the single stalk experiment and in Yager and Schmeeckle (2013) (~18-89 $(cm/s)^2$).

Thus, equation 8 was not previously tested or developed for higher $\langle TKE \rangle$ by Yang and Nepf (2016) or Tanino and Nepf (2008), which is a possible reason why equation 8 underpredicted at higher $\langle TKE \rangle$ and performed better for lower $\langle TKE \rangle$.

Furthermore, there were differences in measurement height above the bed between the single stalk experiments, Yang and Nepf (2016), and Yager and Schmeeckle (2013). Yang and Nepf (2016) measured velocities 1 mm above the bed, while we measured velocities 1 cm above the bed for the single stalk experiments and Yager and Schmeeckle (2013) measured velocities 5 mm above the bed. It is possible that discrepancies in the distance above the bed where velocities were measured could have contributed to the accuracy of $\langle TKE \rangle$ predictions from equation 8. We would expect TKE to generally decrease with greater distance from the bed, which could explain why equation 8 overpredicted TKE for data collected 5 mm from the bed in experiments by Yager and Schmeeckle (2013).

More studies are needed to confirm the accuracy and limitations of U predictions from equations 5 and 7 and $\langle TKE \rangle$ predictions from equation 8, specifically to confirm or expand the range of measured U and $\langle TKE \rangle$ that these equations can be applied to ($U \leq 0.19$ m/s and $\langle TKE \rangle \leq 55$ (cm/s)^2), and to further test their applicability in natural topography. The range of U and $\langle TKE \rangle$ that these equations can be applied to is currently limited to $U \leq 0.19$ m/s and $\langle TKE \rangle \leq 55$ (cm/s)^2 to ensure accurate results.

Flow parameter distributions with vegetation & topography

Equations 5, 7, and 8 were developed for vegetated flat bed conditions but performed reasonably well in predicting U and $\langle TKE \rangle$ for experiments with topography. This could imply that vegetated flat beds and vegetated natural topography experience similar flow conditions and the effects of topography can be neglected in vegetation patches. We instead found the distributions of near-bed flow parameters were impacted by both topography and vegetation and in many cases, the effects of topography cannot be ignored.

The scour hole lowered the proportion of very high $\overline{u}$ values in the scour hole-stalk experiment compared to the flat bed-stalk experiment and lowered mean $\overline{u}$. The scour hole had fairly minimal effects on the Reynolds stress distribution, however it increased the proportion of Reynolds stress near the mode, slightly widened the distribution, and slightly lowered the mean Reynolds stress. Lastly, the scour hole increased the proportion of moderate and high TKEs in the distribution and increased $\langle TKE \rangle$ far more than the presence of the stalk did. Although we tend to assume that vegetation stalks are the driver of increased TKE, these experiments reveal that vegetation induced topography could be the main driver. The presence of the scour hole would likely cause an increase in sediment transport because it increased higher TKE and TKE is known to initiate sediment motion. In other words, a bed with topography has higher TKE than a flat bed, therefore topography likely changes the rate of sediment transport in vegetation.

These results help us understand the relative contributions of vegetation and vegetation induced topography and they indicate that vegetation induced topography does change the distributions of $\overline{u}$, Reynolds stress, and TKE beyond the impact of vegetation alone. Vegetation induced topography had a particularly significant impact on TKE, which indicated that it is important to have natural topography around vegetation when measuring flow distributions (particularly TKE) to be used to predict sediment transport, nutrient transport, and aquatic habitat availability.

Flow parameter distributions with changing vegetation density

TKE probability density distributions from Yager and Schmeeckle (2013) fit a gamma distribution well with only two exceptions, however TKE probability density distributions from the single stalk experiments did not fit a gamma distribution as well. This could be caused by TKE data only fitting a gamma distribution in a vegetation patch with overlapping wakes and not for a bed with a single stalk or no stalk. In other words, it seems like a gamma distribution fits are improved by wake interference within vegetation arrays. Another possible reason could be that the single stalk experiments had a far greater number of datapoints in the distributions compared to experiments by Yager and Schmeeckle (2013) and only had data from within the scour hole, while experiments by Yager and Schmeeckle

(2013) had data from the scour hole and a depositional zone. Interestingly, it appears that TKE data from the scour hole-no stalk experiment fits a gamma distribution better than TKE data from the two single stalk experiments so it's possible that the presence of the scour hole improved the gamma distribution fit. Experiments by Yager and Schmeeckle (2013) had multiple bedforms including scour holes, ridges, and dune like features unlike the single stalk experiments. These differences in bedforms could have produced different TKE distributions compared to the TKE distributions from the single stalk experiments, which may be better represented by a gamma distribution.

We were only able to fit TKE data to a gamma distribution and more research is needed to identify another suitable distribution for near-bed velocities and Reynolds stresses. With the exception of ϕ = 0.013, the slopes of the best fit lines for the α - U relation (Figure 6) for the TKE distributions were similar, however the data had significant vertical spread between different vegetation densities and did not collapse into one relation because we did not incorporate vegetation density into the relation. More data are needed to confirm the relations in Figure 6, particularly for ϕ = 0.013 experiments of Yager and Schmeeckle, as we are relying on three or four points per ϕ value to obtain a best fit line. We cannot fully explain why the ϕ = 0.013 case behaved differently from the other vegetation densities. Adding more locations for velocity measurements in experiments by Yager and Schmeeckle (2013) could have helped to better quantify α because they conducted relatively a limited number of transects compared to the single stalk experiments. Perhaps with more data points from each vegetation density, more spatial data to improve the gamma distribution fits, and additional vegetation densities, we could identify one multiple regression relation between α, U and ϕ to better predict the distribution of TKE. As the TKE distribution changes with increasing U according to the α - U relation, the proportion of high TKEs would increase causing higher rates of sediment transport than otherwise expected if using $\langle TKE \rangle$.

Using the same experiments, Yager and Schmeeckle (2013) already determined that sediment transport predictions were more accurate when using the distribution of near-bed Reynolds stresses rather than a single representative shear stress. However, recent studies have suggested that using $\langle TKE \rangle$ may provide better predictions of sediment transport through

vegetation than using a representative shear stress (e.g., Yang and Nepf, 2016). A simple method that allows researchers to generate TKE distributions to use in sediment transport predictions is therefore needed. The α - U relation could be critical in expanding the accessibility and feasibility of using TKE distributions rather than $\langle TKE \rangle$ (ie. Yang and Nepf, 2016). It can be costly and time consuming to collect enough data to obtain a reliable distribution of TKE in the field because of potentially difficult sampling conditions and inconsistent flows. Therefore, being able to estimate a TKE distribution from U and ϕ could to the use of TKE distributions in sediment transport predictions in a similar way to how shear stress distributions have previously been used (Monsalve et al., 2016; Monsalve et al., 2020; Segura and Pitlick, 2015; Mueller and Pitlick, 2014). We outline the steps in this proposed simple method below. Furthermore, we know that sediment transport rates vary spatially in vegetated flows (Yager and Schmeeckle, 2013; Wu et al., 2021) and using a TKE distribution to calculate sediment transport could help to address prediction inaccuracies associated with these spatial differences.

Equations 5 and 7 estimate U fairly well (see previous section), particularly for low U, and one could use then use this U in equation 8 to obtain $\langle TKE \rangle$, which also produced more accurate predictions for low $\langle TKE \rangle$. Knowing U and $\langle TKE \rangle$, the hypothesized α - U relation could be used to obtain α and β could be calculated as $\beta = \alpha / \langle x \rangle$, where $\langle x \rangle$ in this case is $\langle TKE \rangle$. Now, the distribution of TKE from α and β could be used to obtain a distribution of sediment transport rates using a TKE-based sediment transport equation for vegetation (ie. Yang and Nepf, 2018). Lastly, the spatially averaged transport rate could be calculated from the predicted sediment transport distribution to obtain a single estimate of sediment transport in a studied patch. Note that using $\langle TKE \rangle$ (ie. from equation 8) in the same sediment transport equation would result in a different average sediment transport rate due to the nonlinearity of most sediment transport equations. Specifically, the mean sediment transport rate using $\langle TKE \rangle$, rather than the TKE distribution, might be less than a critical value to calculate zero sediment transport when sediment transport could be occurring in some locations with locally high TKE. Using a distribution of TKE captures the spatial variation in TKE that occurs in river systems and takes high TKEs into effect when calculating a spatially averaged transport rate.

Conclusion

We tested the accuracy of equations that predict mean velocity (U) and spatially averaged near-bed turbulent kinetic energy ($\langle TKE \rangle$) that were developed for vegetated beds with flat bed. We used experiments with vegetation and natural topography from the single stalk experiments and with data from experiments by Yager and Schmeeckle (2013). These equations worked well with some data with natural topography, however the accuracy of these equations was higher for lower measured U and $\langle TKE \rangle$. Furthermore, these equations predicted U more accurately for solid volume fraction ϕ = 0.013 and ϕ = 0.031 and less accurately for ϕ = 0.006, however prediction accuracy of $\langle TKE \rangle$ had no clear relation with ϕ. Overall, these equations for U and $\langle TKE \rangle$ had limited applications for beds with natural topography because the accuracy of predictions of U and $\langle TKE \rangle$ was not consistent throughout the range of measured values of U and $\langle TKE \rangle$.

We also compared the distributions of time-averaged streamwise velocity ($\overline{u}$), Reynolds stress, and turbulent kinetic energy (TKE) from the single stalk experiments. The scour hole increased the proportion of medium $\overline{u}$ values and changed the shape of the $\overline{u}$ distribution. The presence of the scour hole increased moderate and high TKEs and increased the mean more than the stalk did. Lastly, we fit a gamma distribution to TKE data from the single stalk experiments and from experiments by Yager and Schmeeckle (2013) to find a relation between the shape parameter (α) of the gamma distribution and U to easily predict the TKE distribution. We found vegetation density-dependent relations between α and U, however the relation for the ϕ = 0.013 experiment was inconsistent with the other relations and more data is needed to support our findings. Obtaining a reliable relation between α and U is a critical step toward incorporating TKE distributions into sediment transport equations. This would allow for the use of a TKE distribution without relying on expensive and difficult field work and data collection currently required to obtain this distribution. Applications of TKE distributions on sediment transport have been explored in fine sediment systems but future work is needed to assess the feasibility of expanding the use of TKE distributions to suspended or bedload in coarse grain transport.

References

Bennett, S., Pirim, T., & Barkdoll, B. (2002). Using simulated emergent vegetation to alter stream flow direction within a straight experimental channel. *Geomorphology, 44*(1-2), 115-126. https://doi.org/10.1016/s0169-555x(01)00148-9

Boulton, A., Findlay, S., Marmonier, P., Stanley, E., & Valett, H. (1998). THE Functional Significance Of The Hyporheic Zone In Streams And Rivers. *Annual Review Of Ecology And Systematics, 29*(1), 59-81. https://doi.org/10.1146/annurev.ecolsys.29.1.59

Budwig, R., & Goodwin, P. (2012). The Center for Ecohydraulics Research Mountain StreamLab—A facility for collaborative research and education. In *Innovations 2012: World innovations in engineering education and research*. Potomac, MD: iNeer.

Carpenter, S., & Lodge, D. (1986). Effects of submersed macrophytes on ecosystem processes. *Aquatic Botany, 26*, 341-370. https://doi.org/10.1016/0304-3770(86)90031-8

Cienciala, P., & Hassan, M. (2016). Sampling variability in estimates of flow characteristics in coarse-bed channels: Effects of sample size. *Water Resources Research, 52*(3), 1899-1922. https://doi.org/10.1002/2015wr017259

Etminan, V., Ghisalberti, M., & Lowe, R. (2018). Predicting Bed Shear Stresses in Vegetated Channels. *Water Resources Research*, *54*(11), 9187-9206. https://doi.org/10.1029/2018wr022811

Jerolmack, D. (2005). Interactions between bed forms: Topography, turbulence, and transport. *Journal Of Geophysical Research*, *110*(F2). https://doi.org/10.1029/2004jf000126

Kaufmann, P. R., Levine, P., Robinson, E. G., Seeliger, C., and Peck, D. V. (1999). "Surface waters: Quantifying physical habitat in wadeable streams." EPA/620/R-99/003, U.S. EPA Office of Research and Development, Environmental Monitoring and Assessment Program (EMAP), Washington, DC.

King, A., Tinoco, R., & Cowen, E. (2012). A k–ε turbulence model based on the scales of vertical shear and stem wakes valid for emergent and submerged vegetated flows. *Journal Of Fluid Mechanics, 701*, 1-39. https://doi.org/10.1017/jfm.2012.113

Leary, K., & Schmeeckle, M. (2017). The Importance of Splat Events to the Spatiotemporal Structure of Near-Bed Fluid Velocity and Bed Load Motion Over Bed Forms: Laboratory Experiments Downstream of a Backward Facing Step. *Journal Of Geophysical Research: Earth Surface, 122*(12), 2411-2430. https://doi.org/10.1002/2016jf004072

Liu, D., Diplas, P., Fairbanks, J., & Hodges, C. (2008). An experimental study of flow through rigid vegetation. *Journal Of Geophysical Research*, *113*(F4). https://doi.org/10.1029/2008jf001042

Melville, B., & Raudkivi, A. (1977). Flow Characteristics In Local Scour At Bridge Piers. *Journal Of Hydraulic Research, 15*(4), 373-380. https://doi.org/10.1080/00221687709499641

Monsalve, A., Yager, E., Turowski, J., & Rickenmann, D. (2016). A probabilistic formulation of bed load transport to include spatial variability of flow and surface grain size distributions. *Water Resources Research*, *52*(5), 3579-3598. https://doi.org/10.1002/2015wr017694

Monsalve, A., Segura, C., Hucke, N., and Katz, S.: A bed load transport equation based on the spatial distribution of shear stress – Oak Creek revisited, Earth Surf. Dynam., 8, 825–839, https://doi.org/10.5194/esurf-8-825-2020, 2020.

Mueller, E., & Pitlick, J. (2014). Sediment supply and channel morphology in mountain river systems: 2. Single thread to braided transitions. *Journal Of Geophysical Research: Earth Surface*, *119*(7), 1516-1541. https://doi.org/10.1002/2013jf003045

Neary, V., Constantinescu, S., Bennett, S., & Diplas, P. (2012). Effects of Vegetation on Turbulence, Sediment Transport, and Stream Morphology. *Journal Of Hydraulic Engineering*, *138*(9), 765-776. https://doi.org/10.1061/(asce)hy.1943-7900.0000168

Nepf, H. (1999). Drag, turbulence, and diffusion in flow through emergent vegetation. *Water Resources Research*, *35*(2), 479-489. https://doi.org/10.1029/1998wr900069

Nepf, H. (2012). Flow and Transport in Regions with Aquatic Vegetation. *Annual Review Of Fluid Mechanics*, *44*(1), 123-142. https://doi.org/10.1146/annurev-fluid-120710-101048

Nicholas, A. P. (2000). Modelling bedload yield in braided gravel bed rivers. Geomorphology, 36(1-2), 89–106. https://doi.org/10.1016/s0169-555x(00)00050-7

Pollen, N. (2007). Temporal and spatial variability in root reinforcement of streambanks: Accounting for soil shear strength and moisture. *CATENA*, *69*(3), 197-205. https://doi.org/10.1016/j.catena.2006.05.004

Recking, A. (2013). An analysis of nonlinearity effects on bed load transport prediction. Journal of Geophysical Research: Earth Surface, 118(3), 1264–1281. https://doi.org/10.1002/jgrf.20090

Romdhane, H., Soualmia, A., Cassan, L., & Belaud, G. (2018). Effect of vegetation on flows and sediment transport. *E3S Web Of Conferences*, *40*, 02017. https://doi.org/10.1051/e3sconf/20184002017

Rominger, J. T., A. F. Lightbody, and H. M. Nepf (2010), Effects of added vegetation on sand bar stability and stream hydrodynamics, J. Hydraul. Eng., 136, 994–1002, doi:10.1061/(ASCE)HY.1943- 7900.0000215

Rubol, S., Tonina, D., Vincent, L., Sohm, J., Basham, W., & Budwig, R. et al. (2018). Seeing through porous media: An experimental study for unveiling interstitial flows. *Hydrological Processes*, *32*(3), 402-407. https://doi.org/10.1002/hyp.11425

Schmeeckle, M. (2015). The role of velocity, pressure, and bed stress fluctuations in bed load transport over bed forms: numerical simulation downstream of a backward-facing step. *Earth Surface Dynamics*, *3*(1), 105-112. https://doi.org/10.5194/esurf-3-105-2015

Segura, C., & Pitlick, J. (2015). Coupling fluvial-hydraulic models to predict gravel transport in spatially variable flows. *Journal Of Geophysical Research: Earth Surface*, *120*(5), 834-855. https://doi.org/10.1002/2014jf003302

Simon, A., & Collison, A. (2002). Quantifying the mechanical and hydrologic effects of riparian vegetation on streambank stability. *Earth Surface Processes And Landforms*, *27*(5), 527-546. https://doi.org/10.1002/esp.325

Tanino, Y., & Nepf, H. (2007), Experimental investigation of lateral dispersion in aquatic canopies, paper presented at 32nd Congress-International Association for Hydraulic Research, p. 152, Venice, Italy, 1–6 Jul.

Tanino, Y., & Nepf, H. (2008). Lateral dispersion in random cylinder arrays at high Reynolds number. *Journal Of Fluid Mechanics*, *600*, 339-371. https://doi.org/10.1017/s0022112008000505

Tinoco, R., San Juan, J., & Mullarney, J. (2020). Simplification bias: lessons from laboratory and field experiments on flow through aquatic vegetation. *Earth Surface Processes And Landforms*, *45*(1), 121-143. https://doi.org/10.1002/esp.4743

Vargas-Luna, A., Crosato, A., & Uijttewaal, W. (2014). Effects of vegetation on flow and sediment transport: comparative analyses and validation of predicting models. *Earth Surface Processes And Landforms*, *40*(2), 157-176. https://doi.org/10.1002/esp.3633

Yager, E., & Schmeeckle, M. (2013). The influence of vegetation on turbulence and bed load transport. *Journal Of Geophysical Research: Earth Surface*, *118*(3), 1585-1601. https://doi.org/10.1002/jgrf.20085

Yang, J., & Nepf, H. (2018). A Turbulence-Based Bed-Load Transport Model for Bare and Vegetated Channels. *Geophysical Research Letters*, *45*(19). https://doi.org/10.1029/2018gl079319

Yang, J., Chung, H., & Nepf, H. (2016). The onset of sediment transport in vegetated channels predicted by turbulent kinetic energy. *Geophysical Research Letters*, *43*(21). https://doi.org/10.1002/2016gl071092

Yang, J., Kerger, F., & Nepf, H. (2015). Estimation of the bed shear stress in vegetated and bare channels with smooth beds. *Water Resources Research*, *51*(5), 3647-3663. https://doi.org/10.1002/2014wr016042

Wang, C., Zheng, S., Wang, P., & Hou, J. (2015). Interactions between vegetation, water flow and sediment transport: A review. *Journal Of Hydrodynamics*, *27*(1), 24-37. https://doi.org/10.1016/s1001-6058(15)60453-x

Wu, H., Cheng, N., & Chiew, Y. (2021). Bed-Load Transport in Vegetated Flows: Phenomena, Parametrization, and Prediction. *Water Resources Research*, *57*(4). doi: 10.1029/2020wr028143